Structural Characterization and Biological Fluid Interaction of Sol−Gel-Derived Mg-Substituted Biphasic Calcium Phosphate Ceramics

S. Gomes,[†,‡] G. Renaudin,[†] E. Jallot,[‡] and J.-M. Nedelec*[,†]

Laboratoire des Matériaux Inorganiques, CNRS UMR 6002, Université Blaise Pascal & Ecole Nationale Supérieure de Chimie de Clermont-Ferrand, Clermont Université, 24 avenue des Landais, 63177 Aubière Cedex, France, and Laboratoire de Physique Corpusculaire de Clermont-Ferrand, CNRS/IN2P3 UMR 6533, Université Blaise Pascal, Clermont Université, 24 avenue des Landais, 63177 Aubière Cedex, France

ABSTRACT Sol−Gel chemistry has been used to prepare undoped and Mg-substituted biphasic calcium phosphate (BCP) ceramics composed of hydroxyapatite (HAp) and whitlockite (β-TCP) phases. Different series of samples have been synthesized with different Mg-doping levels (from 0 to 5 atomic % of Ca atoms substituted) and different temperatures of calcination (from 500 to 1100 °C). All of the powdered samples were systematically treated by Rietveld refinement to extract the quantitative phase analysis and the structural and microstructural parameters, to locate the Mg crystallographic sites, and to refine the composition of the Mg-substituted phases. The temperature dependence of the weight amount ratio between HAp and β-TCP is not monotonic because of the formation of minor phases such as $Ca_2P_2O_7$, CaO, MgO, and $CaCO_3$ and certainly an amorphous phase. On the other hand, the Mg stabilizing feature on the β-TCP phase has been evidenced and explained. The mechanism of stabilization by small Mg^{2+} is different from that by large Sr^{2+}. Nevertheless, in both cases, the β-TCP stabilization is realized by an improvement of the environment of the Ca4 site unusually face-coordinated to a PO_4 tetrahedron. The substitution of a Mg atom in the Ca5 site allows considerable improvement of the bond valence sum of the unusual Ca4 polyhedron. The temperatures of calcination combined with the amount of Mg atoms introduced allow monitoring of the phase composition of the BCP ceramics as well as their microstructural properties. The bioactivity properties of the BCP samples are improved by the presence of Mg atoms in the structure of the β-TCP phase. The mechanism of improvement is mainly attributed to an accelerated kinetic of precipitation of a calcium phosphate layer at the surface comprising HAp and/or β-TCP phases.

KEYWORDS: biomaterials • biointerfaces • biomineralization • calcium phosphates

1. INTRODUCTION

Biphasic calcium phosphate (BCP) ceramics, composed of a mixture of hydroxyapatite [HAp, $Ca_5(PO_4)_3OH$] and β-tricalcium phosphate or whitlockite [β-TCP, β-$Ca_3(PO_4)_2$], are interesting candidates in reconstructive surgery. Bone mineral mass is dominated by nanocrystalline nonstoichiometric HAp (1−3). For these reasons, HAp has been widely used as biocompatible materials for permanent bone replacement and scaffolds for new bone growth or for bone prostheses coating (4). β-TCP has also been largely considered because of its high solubility, in particular in conjunction with HAp to produce the so-called BCP. Advantages of BCP ceramics are the difference in dissolution properties of the two phases, the rapid bone reconstruction around the implant site, and their close matches with the inorganic components of bones (5−7). The addition of Mg (the fourth highest concentrated cation in the human body after Ca, K, and Na) in BCP is attracting attention because of the beneficial effects on the physicochemical properties of minerals (8−10) and on the bone metabolism (2, 11, 12). Bone minerals contain various amounts of Mg (13), either adsorbed at the surface of HAp crystals or incorporated inside its crystallographic structure (12). The mineral encountered in biological systems commonly named with the term "whitlockite" (in the biological and medical literature) is, in fact, a Mg-substituted β-TCP phase (2, 14−17). The deficiency of Mg in bone has been suggested as a possible risk factor for osteoporosis in humans (11). Mg is known to reduce the degradation rate of calcium phosphate biomaterials (18−20) and to influence the crystallization of mineral substances (12, 13, 21−27). The substituted low-Mg-containing apatite sample decreased the osteoinductive properties of biomaterials, whereas the substituted high-Mg-containing apatite had a toxic effect on bone cells (12). In recent years, the development of Mg-substituted HAp and/or BCP ceramics has been a subject of interest (10, 28−30). The amount of HAp and β-TCP in BCP can be tailored by the temperature of calcination (31, 32) as well as by the insertion of Mg (2, 10, 21, 33, 34) or Sr

* Corresponding author. Tel: 00 33 4 73 40 7195. Fax 00 33 4 73 40 53 28. E-mail: j-marie.nedelec@univ-bpclermont.fr.
Received for review November 4, 2008 and accepted December 29, 2008
† Laboratoire des Matériaux Inorganiques, CNRS UMR 6002.
‡ Laboratoire de Physique Corpusculaire de Clermont-Ferrand, CNRS/IN2P3 UMR 6533.
DOI: 10.1021/am800162a

Table 1. Nominal and Experimental (Determined by ICP-AES) Composition (wt %) of Ca, P, and Mg in the Synthesized Samples

	nominal composition				experimental composition			
sample	Ca	P	Mg	substitution level (%)	Ca	P	Mg	substitution level (%)
00Mg series	39.90	18.50	0	0	41.89	18.05	0	0
05Mg1100	39.73	18.51	0.12	0.50	40.48	18.83	0.13	0.52
10Mg1100	39.56	18.53	0.24	1.00	40.24	18.89	0.25	1.03
20Mg1100	39.22	18.56	0.49	2.00	40.27	18.70	0.49	1.97
50Mg series	38.20	18.65	1.22	5.00	38.08	19.55	1.16	4.77

(35, 36). The dissolution properties of both phases can be modified by the incorporation of doping elements (37). The substitution of Mg during the preparation process of BCP ceramics can also be useful for monitoring the microstructural parameters (namely, the average crystallite size) of HAp and β-TCP (10, 13, 21−27). The purpose of our study was to examine in detail the incorporation of Mg^{2+} ions in BCP samples at the atomic level: identification and quantification of the crystallized phases, identification of the Mg-occupied crystallographic sites, determination of the chemical composition of the different phases, and determination of the microstrucral parameters (average crystallite size and internal constraints). Rietveld analyses were performed on powder X-ray diffraction (PXRD) patterns recorded from a series of BCP samples containing different amounts of Mg [from 0 to 5 atomic % (at. %) of Ca substituted by Mg] and with different temperatures of calcination (from 500 to 1100 °C).

2. EXPERIMENTAL SECTION

2.1. Sol−Gel Elaboration of Mg-Substituted BCP. The sol−gel route previously proposed by the authors (38, 39) was used. Briefly, to produce 2 g of pure HAp powder, 4.7 g of $Ca(NO_3)_2 \cdot 4H_2O$ (Aldrich, USA; purity = 99%) and 0.84 g of P_2O_5 (Avocado Research Chemicals, Ltd., U.K.; purity = 99%) were dissolved in ethanol under stirring and refluxed at 85 °C for 24 h to favor nucleation. Then, this solution was kept at 55 °C for 24 h to obtain a white consistent gel and further dried at 80 °C for 10 h to obtain a white powder. Finally, the powder was heated at 1100 °C for 15 h (the obtained sample was named 00Mg1100). To prepare Mg-substituted HAp, the required amount of $Mg(NO_3)_2 \cdot 6H_2O$ (Aldrich, USA; purity = 99.999%) was added to the solution. Four Mg-substituted samples were prepared with Mg substitution levels of 0.5, 1, 2, and 5 at. % of Ca substituted by Mg atoms, respectively noted as 05Mg1100, 10Mg1100, 20Mg1100, and 50Mg1100 samples.

Furthermore, the pure HAp samples (named the 00Mg series) of nominal composition $Ca_5(PO_4)_3 \cdot OH$ and 5 at. % Mg-doped HAp samples (named the 50Mg series) have been synthesized with calcination temperatures of 500, 700, 800, 900, and 1000 °C. Samples are noted respectively as 00Mg500, 00Mg700, 00Mg800, 00Mg900, and 00Mg1000 for the pure 00Mg series and 50Mg500, 50Mg700, 50Mg800, 50Mg900, and 50Mg1000 for the 50Mg series.

The chemical compositions of all samples were determined by inductively coupled plasma atomic emission spectrometry (ICP-AES). The nominal and experimental compositions of the 00Mg series, 05Mg1100, 10Mg1100, 20Mg1100, and 50Mg series are listed in Table 1. As is usually observed for sol−gel-derived ceramics (40), the global nominal compositions have been achieved pretty well.

2.2. PXRD. PXRD patterns were recorded on a X'Pert Pro Philips diffractometer, with $\theta-\theta$ geometry, equipped with a solid detector X-Celerator and using Cu Kα radiation (λ = 1.541 84 Å). PXRD patterns were recorded at room temperature in the interval $3° < 2\theta < 120°$, with a step size of $\Delta 2\theta = 0.0167°$ and a counting time of 200 s for each data value. A total counting time of about 200 min was used for each sample. A Si PXRD pattern was collected (from pure Si standard) by using the same experimental conditions in order to extract the instrumental resolution function. The quality of the measured PXRD patterns with good statistical counting and good signal/background ratios allowed one to perform quantitative Rietveld analyses by taking into account minor crystallized phases, i.e., below 1 wt %.

2.3. Rietveld Refinements. PXRD pattern were analyzed by Rietveld refinement with *FullProf.2k* (41). According to the calcination temperature and the Mg-doping level, the following phases have been observed: HAp, β-TCP, calcite $CaCO_3$, lime CaO, periclase MgO, and the two dicalcium diphosphate polymorphs (α-$Ca_2P_2O_7$ and β-$Ca_2P_2O_7$). The initial structural parameters used for the Rietveld analyses were the following. The structural parameters of HAp, $Ca_5(PO_4)_3 \cdot OH$, were taken from ref 42: space group $P6_3/m$, $Z = 2$, $a = 9.4218$ Å, $c = 6.8813$ Å, 7 independent atomic positions of two Ca, one P, and four O positions. The O4 oxygen position (i.e., the hydroxyl anion) is half-occupied; this corresponds to a statistically disordered 4e position shifted around the 2a (0, 0, $^1/_4$) site. The structural parameters of β-TCP, β-$Ca_3(PO_4)_2$, were taken from ref 43: space group $R3c$, $Z = 21$, $a = 10.4352$ Å, $c = 37.4029$ Å, 18 independent atomic positions of 5 Ca, 3 P, and 10 O positions. The Ca5 calcium position has a partial occupancy factor. The structural parameters of lime, CaO (respectively periclase, MgO), were taken from ref 44 (respectively ref 45): space group $Fm\bar{3}m$, $Z = 4$, $a = 4.8071$ Å (respectively $a = 4.22$ Å). The structural parameters of calcite, $CaCO_3$, were taken from ref 46: space group $R\bar{3}c$, $Z = 6$, $a = 4.9910$ Å, $c = 16.9719$ Å. The structural parameters of α-$Ca_2P_2O_7$ were taken from ref 47: space group $P2_1/n$, $Z = 4$, $a = 12.66$ Å, $b = 8.542$ Å, $c = 5.315$ Å, $\beta = 90.3°$, 11 independent atomic positions of two Ca, two P, and seven O positions. The structural parameters of β-$Ca_2P_2O_7$ were taken from ref 48: space group $P4_1$, $Z = 8$, $a = 6.6858$ Å, $c = 24.147$ Å, 22 independent atomic positions of 4 Ca, 4 P, and 14 O positions. In a first step, all of the structural parameters were fixed to the literature values. Then during the successive refinement cycles, numerous parameters were allowed to vary according to the relative weight amounts of the observed phases. The following refinement sequence was used: first lattice parameters, zero shift and peak profiles; next atomic parameters, positional, isotropic temperature, and occupancy factors. The scattering contrast between Ca and Mg atoms allowed the refinement of the substitution by Mg in the different Ca sites for the main phases. The last refinement cycles were performed by introducing a H atom from the hydroxyl anion. The H4 (atom labels taken from ref 42 in all of the text) position was located on the site 4e, a soft constraint of 0.92 ± 0.05 Å was applied to the distance O4−H4, and the isotropic temperature factors of H4 were constrained to be 1.2 times B_{iso} of the corresponding oxygen atom O4, as is usual for hydroxyl groups (49−51). The use of the instrumental resolution function improved the peak profile modeling while decreasing the number of profile parameters. It allowed also the extraction of the sample intrinsic microstructural parameters: average apparent crystallite size and average maximum strain. The diffraction profiles (both instrumental and sample intrinsic) were modeled by using a Thomson−Cox−Hastings pseudo-Voigt function (41). Refinement with the anisotropic line broadening procedure (41) was used to calculate the anisotropy of morphology of the HAp crystallites. As indicated in ref 35, care was taken to obtain accurate values for the quantitative phase analyses. An example of a Rietveld plot can be found in the Supporting Information for the 50Mg700 sample. Table 2 gathers the refined lattice

Table 2. Results of the Quantitative Phase Analyses Using the Rietveld Method and Refined Lattice Parameter of the HAp and β-TCP Phases[a]

sample			HAp			β-TCP								
label	Mg[b] at. %	T (°C)	wt %[c]	a (Å)	c (Å)	wt %[c]	a (Å)	c (Å)	α-$Ca_2P_2O_7$ (wt %)[c]	β-$Ca_2P_2O_7$ (wt %)[c]	CaO (wt %)[c]	$CaCO_3$ (wt %)[c]	MgO (wt %)[c]
00Mg500	0.0	500	93.0(2)	9.43471(9)	6.88173(9)				2.88 (4)		2.35(2)	1.79(3)	
00Mg700	0.0	700	84.7(2)	9.42210(8)	6.88582(6)	3.27(6)	10.4412(5)	37.419(2)	8.47 (9)		2.86(2)	0.73(2)	
00Mg800	0.0	800	82.0(2)	9.42327(4)	6.88490(3)	9.8(1)	10.4408(2)	37.4106(7)		3.13(6)	5.08(4)		
00Mg900	0.0	900	71.6(2)	9.42376(3)	6.88367(3)	24.0(1)	10.44016(9)	37.4007(4)		0.65(6)	3.69(2)		
00Mg1000	0.0	1000	75.7(2)	9.42461(1)	6.88415(2)	20.2(2)	10.4403(1)	37.4033(5)			4.10(3)		
00Mg1100	0.0	1100	91.7(2)	9.42454(2)	6.88429(2)	1.11(4)	10.4412(5)	37.401(3)			7.14(3)		
05Mg1100	0.5	1100	87.3(3)	9.42456(2)	6.88434(2)	12.2(2)	10.4241(2)	37.3883(9)			0.39(2)		0.11(2)
10Mg1100	1.0	1100	76.4(2)	9.42414(2)	6.88448(2)	22.4(2)	10.4218(1)	37.3775(4)			0.89(2)		0.28(2)
20Mg1100	2.0	1100	63.1(2)	9.42447(2)	6.88450(2)	35.2(2)	10.41224(7)	37.3643(3)			1.21(2)		0.46(2)
50Mg500	5.0	500	84.6(3)	9.41791(8)	6.88214(7)	13.2(1)	10.3653(5)	37.220(2)			0.34(2)	1.00(4)	0.89(3)
50Mg700	5.0	700	77.3(2)	9.42316(7)	6.88619(6)	16.1(1)	10.3642(4)	37.231(2)	5.04(6)		0.55(1)	0.66(3)	0.36(2)
50Mg800	5.0	800	75.8(2)	9.42390(4)	6.88600(3)	16.1(1)	10.3745(2)	37.2874(8)		6.11(6)	0.82(1)		1.15(2)
50Mg900	5.0	900	60.6(2)	9.42558(3)	6.88615(3)	37.0(1)	10.38257(7)	37.3107(3)		0.87(5)	0.47(1)		1.03(2)
50Mg1000	5.0	1000	67.8(2)	9.42521(3)	6.88578(2)	29.9(1)	10.38702(8)	37.2930(4)		0.47(5)	0.48(2)		1.34(3)
50Mg1100	5.0	1100	30.0(1)	9.42402(4)	6.88541(3)	69.5(2)	10.38506(6)	37.3060(3)					0.46(2)

[a] Standard deviations are indicated in parentheses. [b] The Mg at. % value corresponds to the Ca atomic percent substituted by Mg. [c] Weight percent.

parameter values of HAp and β-TCP, as well as the refined relative weight amounts (wt %) of the observed crystallized phases for each sample. Microstructural parameters of HAp, details on the localization and the amount of Mg in the different Mg-doped samples, and structural parameters of the Mg-doped β-TCP phases with composition $Ca_{2.841(9)}Mg_{0.159(9)}(PO_4)_2$ from the 50Mg1100 sample can be found in the Supporting Information (Tables SI1−SI3, respectively).

2.4. Interaction with Biological Fluid. The Mg-substituted powdered samples (16 mg) were immersed at 37 °C for 1, 2, 5, 10, and 20 days in 24 mL of a standard Dulbecco's Modified Eagle Medium (DMEM; VWR International SAS, France); pH 7.3. DMEM contained the following mineral ingredients: NaCl (6400 mg · L^{-1}), KCl (400 mg · L^{-1}), $CaCl_2$ (200 mg · L^{-1}), $MgSO_4 \cdot 7H_2O$ (200 mg · L^{-1}), NaH_2PO_4 (124 mg · L^{-1}), and $NaHCO_3$ (3700 mg · L^{-1}). DMEM has been considered rather than simulated body fluid because it matches more closely the biological conditions in particular due to the presence of amino acids. DMEM is also the culture medium that will be used for future cell interaction studies. At each immersion time, the concentrations of the three elements Ca, P, and Mg were determined by ICP-AES in the biological fluid after elimination of the solid by centrifugation.

3. RESULTS AND DISCUSSION

3.1. Effect of the Temperature of Calcination on the Mg-Free BCP Series (i.e., the 00Mg Series). The PXRD patterns of the 00Mg series (i.e., samples 00Mg500, 00Mg700, 00Mg800, 00Mg900, 00Mg1000, and 00Mg1100) can be found in the Supporting Information (Figure SI2). All of these PXRD patterns are mainly composed of diffraction peaks of the HAp phase (see the stars in Figure SI2 of the Supporting Information). Clear evidence of an increase of the crystallinity when the temperatures of calcination increase is given by the evolution of the diffraction peak widths. The main phases are the expected HAp and β-TCP phases, and minor crystallized phases are α- and β-$Ca_2P_2O_7$, CaO, and $CaCO_3$ (Table 2). In agreement with the literature, the α-$Ca_2P_2O_7$ phase observed at 500 and 700 °C is transformed into the β-$Ca_2P_2O_7$ polymorph at 800 °C (temperature of transition of about 750 °C) (47, 48, 52, 53). This dicalcium diphosphate phase disappeared at 1000 °C. The calcite phase observed in the samples calcined at 500 and 700 °C disappeared in the sample calcined at 800 °C and above, in agreement with its temperature of decomposition of the carbonate of around 750 °C (54). The amount of lime (CaO) is dependent on the reaction transformation between the three phosphate phases: HAp (ratio Ca/P = 1.67), β-TCP (ratio Ca/P = 1.5), and $Ca_2P_2O_7$ (ratio Ca/P = 1.0). From 500 to 900 °C, an increase of the lime weight percent is observed simultaneously with a decrease of the HAp weight percent, an increase of the β-TCP and $Ca_2P_2O_7$ weight percents, and a disappearance of $CaCO_3$ due to the following reactions (Table 2 and Figure 1a):

$$2Ca_5(PO_4)_3OH \rightarrow 3Ca_3(PO_4)_2 + CaO + H_2O \quad (1)$$

$$2Ca_5(PO_4)_3OH \rightarrow 3Ca_2P_2O_7 + 4CaO + H_2O \quad (2)$$

$$CaCO_3 \rightarrow CaO + CO_2 \quad (3)$$

At 1000 °C, and even more at 1100 °C, stabilization of the HAp phase is observed (Figure 1a) simultaneously with an increase of the weight percent of CaO in disagreement with reactions (1) and (2). The increase of the CaO amount should be attributed either to the presence of an amorphous phase or to the nonstoichiometry of the HAp phase at high temperature. Refinements of the site occupancy factors for the calcium and hydroxide sites in the HAp structure did not evidence a nonstoichiometry. All of the refined occupancy parameters were very close to a full site filling, in agreement with the literature, which indicates that the HAp phase is stoichiometric (with a Ca/P ratio of 1.67) when calcined above the temperature of 700 °C (10, 31, 32).

Lattice parameters of HAp and β-TCP are not temperature-dependent (Table 2 and Figure 1b). On the contrary,

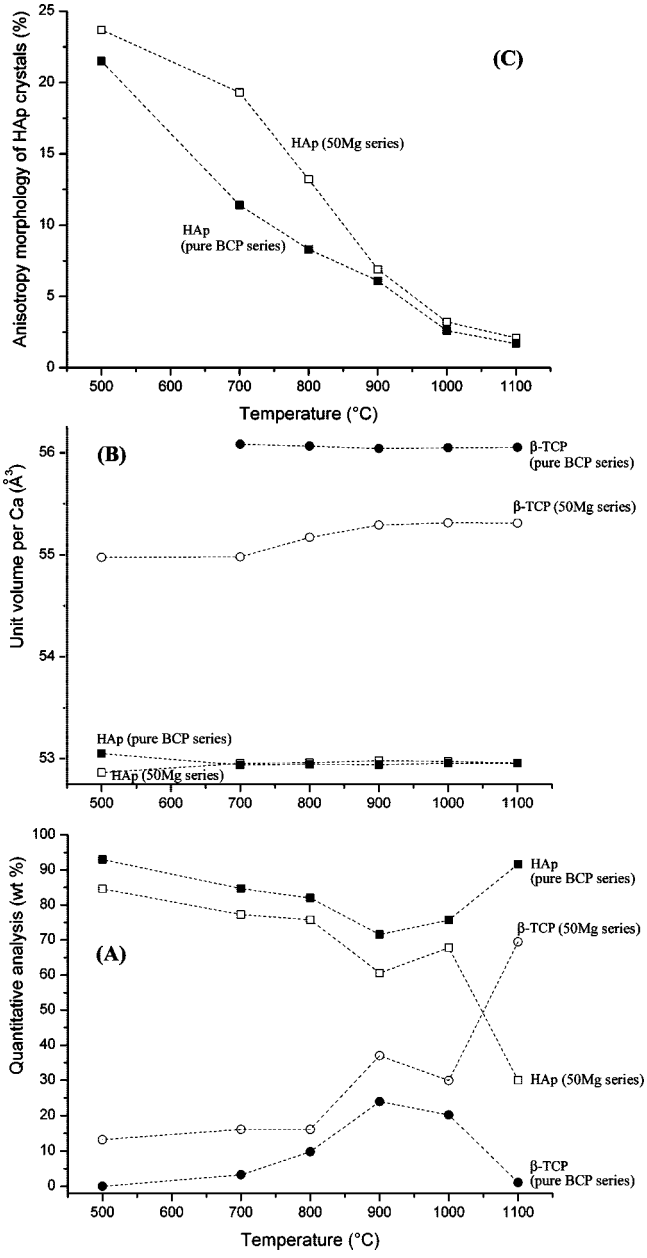

FIGURE 1. Rietveld refinement results as a function of the temperature: (A) quantitative phase analysis; (B) unit volume per Ca = unit cell volume/number of Ca atoms per cell; (C) anisotropy of the HAp crystal morphology = $(Lc_{[110]} - Lc_{[001]})/2\langle Lc\rangle \times 100$ (Lc = coherent domain length; see Table SI1 of the Supporting Information). Results are represented for the HAp (squares) and β-TCP (circles) phases. Filled (respectively open) symbols are relative to the pure BCP series (respectively 5% Mg-doped BCP series). Dashed lines are only guides for the eyes.

temperature dependence is observed for the anisotropy of the HAp crystallites morphology (Figure 1c), for the HAp and β-TCP coherent domain sizes, and for HAp and β-TCP average maximum strains (Table SI1 of the Supporting Information). Unit volumes per Ca atom are represented in Figure 1b in order to compare directly the behavior of HAp (unit cell volume of about 530 Å^3 with 10 Ca atoms per cell) and β-TCP (unit cell volume of about 3530 Å^3 with 63 Ca atoms per cell) phases. The unit cell volume of the HAp heated at 500 °C is quite a bit larger (about 0.2%) than the unit cell volumes measured for the HAp heated between 700 and 1100 °C (unit cell volume of about 529.5 Å^3). The unit cell volume of β-TCP (about 3531.1 Å^3, close to the published value of 3527.26 Å^3 (43)) is also invariant with the temperature of calcination. Upon heating, an important increase of the coherent domain sizes (from about 500 Å at 500 °C to more than 2000 Å at 1100 °C) for both HAp and β-TCP phases and a clear decrease of the average maximum strains (from 2.0% at 500 °C to 0.1% at 1100 °C) for the HAp phase are observed. Microstructural parameter refinements indicate a needlelike morphology for the HAp crystals, elongated along the hexagonal axis (Figure 1c), as was already mentioned (2). The anisotropy of the HAp crystallite morphology decreases regularly when the temperature of calcination increases (Figure 1c). HAp crystallites become tabular above a calcination temperature of 1000 °C. The different crystallite morphologies of samples calcined at 500 and 1100 °C are shown in Figure 2.

3.2. Effect of the Temperature of Calcination on the 5% Mg-Doped BCP Series. Figure 3 displays a detail (2θ range from 20° to 60°) of the PXRD patterns of the 50Mg series (i.e., samples 50Mg500, 50Mg700, 50Mg800, 50Mg900, 50Mg1000, and 50Mg1100). All of these PXRD patterns are mainly composed of the diffraction peaks of the HAp phase (see the stars in Figure 3), except for the 50Mg1100 PXRD pattern, in which the β-TCP contribution became predominant (see the circles in Figure 3). As well as the Mg-free BCP series, an increase of the crystallinity is observed when the temperature of calcination increases. Minor crystallized phases are α- and β-$Ca_2P_2O_7$, CaO, $CaCO_3$, and also MgO, which presents relatively broad diffraction peaks (Table 2). The presence of Mg in the sample seems not to affect the transition temperature from the α-$Ca_2P_2O_7$ polymorph to the β-$Ca_2P_2O_7$ polymorph, which was still observed between 700 and 800 °C (47, 48, 52, 53). The amount of lime in the 50Mg series is clearly inferior to that observed previously in the pure BCP series. Lime is associated with a quite equivalent weight amount of periclase (MgO), i.e., around 1 wt % for both alkaline-earth oxide phases. Nevertheless, we can observe a light increase of the weight amount of lime and periclase from 500 to 800 °C (the same evolution already observed in the pure BCP series) followed by a decrease of these weight amounts up to 1100 °C (in contrast with the pure BCP series, for which the weight amount of lime was maximal at 1100 °C). The main difference observed between the two series (Mg-free BCP and 50Mg series) is the clear stabilization of the β-TCP phase in the presence of Mg at 1100 °C. Between 500 and 1000 °C, the two series show quite the same evolution of their quantitative phase analyses. Also, they completely invert the ratio HAp/β-TCP at 1100 °C (Table 2 and Figure 1a). The stabilization of the β-TCP phase does not correlate with the disappearance of lime at 1100 °C, which disagrees again with reaction (1). Then, the presence of an amorphous phase, as identified in a previous study on Sr-doped HAp samples (35), should be considered. ICP-AES measurements indicate that the experimentally introduced MgO amounts agree with the expected nominal values (Tables 1). The total

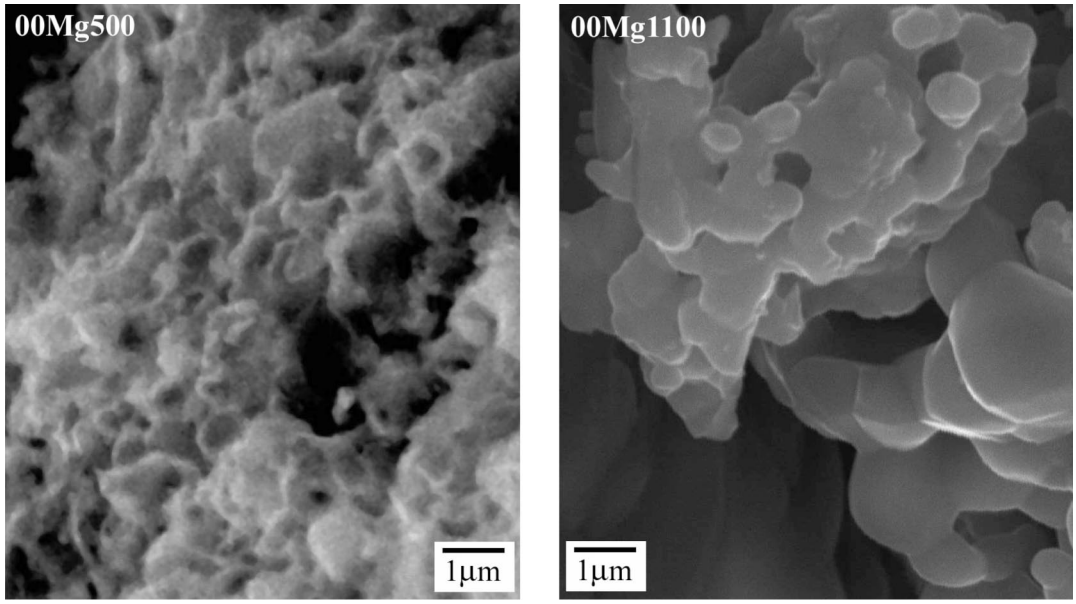

FIGURE 2. Representative scanning electron microscopy images of Mg-free sol−gel BCP samples calcined at 500 °C (left) and 1100 °C (right).

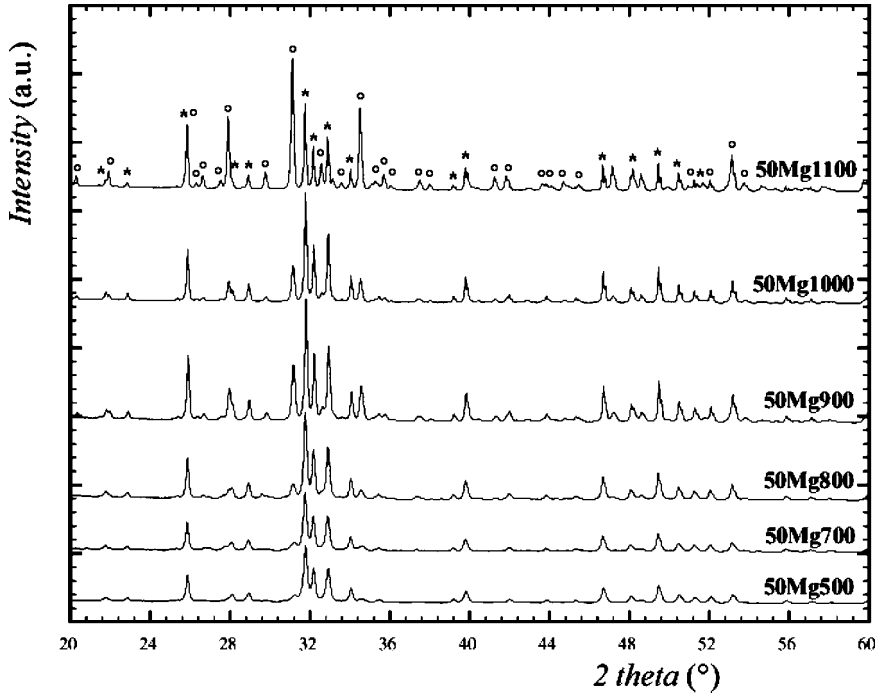

FIGURE 3. Details of the PXRD patterns (in the range $20 < 2\theta < 60°$) from the 50Mg series with calcination temperatures from 500 to 1100 °C. The marks * and ○ indicate the main diffraction peaks of respectively the HAp and β-TCP phases.

amounts of refined magnesium oxide (MgO from periclase and from the Mg-substituted β-TCP phase) are also in quite good agreement with the expected nominal values for samples calcined at 1100 °C (see Table SI2 of the Supporting Information). Nevertheless, samples from the 50Mg series calcined at a temperature below 900 °C show a deficiency in the refined MgO amount, proving the presence of an amorphous phase with a temperature-dependent weight amount.

Refined lattice parameters (Table 2 and Figure 1b) indicate clearly that Mg insertion occurs in the β-TCP phase. The unit cell volume of β-TCP from the 50Mg1100 sample is about 3484.4 Å^3 (a decrease of 1.3% compared to the value of about 3531.1 Å^3 for the Mg-free BCP series), close to the value of 3496.04 Å^3 for the referenced Mg-substituted β-TCP $Mg_{0.11}Ca_{2.89}(PO_4)_2$ (34). The heating from 500 to 900 °C extracts Mg atoms from the β-TCP structure, as shown by the increase of the corresponding unit cell volumes (from 3463.20 Å^3 at 500 °C to 3483.14 Å^3 at 900 °C) and the decrease of the refined Mg occupancies in Ca sites (x refined value from 0.23 at 700 °C to 0.12 at 900 °C in the $Ca_{3-x}Mg_x(PO_4)_2$ solid solution). The increase of the β-TCP unit cell mainly occurs above 700 °C and is correlated with the evolution of the refined Mg amounts in the Ca5 site in the

β-TCP structure (Table SI2 and Figure SI3 of the Supporting Information). On the other hand, the HAp unit cell volume did not show significant evolution when increasing the temperature of calcination. No difference is observed between the Mg-free and 50Mg series. The same unit cell volumes were observed for HAp from the pure series (529.554 Å^3 when calcined at 1100 °C) and HAp from the 50Mg series (529.582 Å^3 when calcined at 1100 °C). The only weak difference is observed for the temperature of calcination of 500 °C: HAp unit cell volume of 528.645 Å^3 in the 5% Mg series and 530.500 Å^3 in the Mg-free series. The decrease of about 0.35% could indicate a small amount of Mg substitution in the HAp structure for 500 °C calcination. At 700 °C and above, this small amount of substituted Mg atoms in the HAp phase is extracted (simultaneously with an increase of the crystallinity). The microstuctural parameters refined from the samples of this 50Mg series are related to those from the Mg-free series: the same order of crystallite size, crystal shape, and average maximum strain (Figure 1c).

3.3. Effect of the Mg-Doping Amount in the BCP Series Calcined at 1100 °C. Table 2 and Figure SI4 of the Supporting Information show the evolution observed when Mg atoms are introduced during synthesis in our BCP samples. The known stabilization effect of Mg on the β-TCP phase (10, 29) is here clearly evidenced and characterized (Table 2 and Figure SI4a of the Supporting Information). The weight amount of β-TCP is quite linearly dependent on the amount of Mg atoms introduced during the synthesis (and inversely for HAp). A mixture of 50 wt % of HAp and 50 wt % of β-TCP is obtained for an introduced Mg of about 3 at. %, whereas a quite pure HAp sample is formed when no Mg atoms are introduced. Evolution of the lattice parameters (Table 2 and Figure SI4b of the Supporting Information) indicates that Ca atoms are substituted by Mg in the β-TCP, and not in the HAp phase. The more Mg atoms that were introduced, the more the unit cell volume of β-TCP decreased. The unit cell volume of the HAp phase is not sensitive to the introduction of Mg atoms during the synthesis. Figure 4 represents Vegard's law relative to the $Ca_{3-x}Mg_x(PO_4)_2$ solid solution in the range $0.0 < x < 0.3$. This solid solution is limited (with $x < 1.5$), as shown by the monoclinic *C*2/*c* symmetry of the compound stanfieldite $Ca_{1.5}Mg_{1.5}(PO_4)_2$ (56). The unit cell volume/refined composition ratios of our samples (the stars in Figure 4) correlate fairly well with a linear Vegard's law fitted from the referenced values (circles and linear fit in Figure 4) (34, 43). Only the position of the sample 05Mg1100 diverges from the linear fit. No Mg atom was found in this sample during the Rietveld refinement, while the refined unit cell volume corresponds to an *x* value close to 0.03. This discrepancy is attributed to the low amount of β-TCP in the 05Mg1100 sample (i.e., less than 15 wt %), leading to a not very stable refinement of its structural parameters.

3.4. Structural Site Localization of Mg Atoms in the BCP Samples. During the last cycles of refinement, attempts were performed to localize Mg atoms in all of the Ca sites describing HAp (two nonequivalent Ca sites repre-

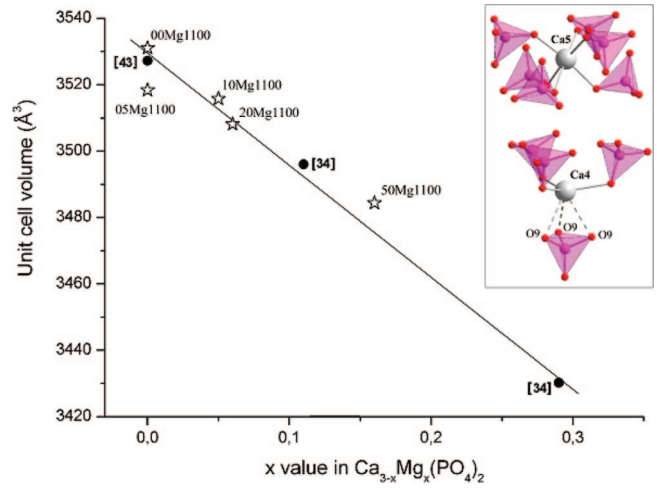

FIGURE 4. Representation of Vegard's law for the $Ca_{3-x}Mg_x(PO_4)_2$ solid solution for $0.0 < x < 0.3$. Closed circles, with the corresponding linear fit, correspond to the literature values (see ref 43 for $x = 0.0$ and ref 34 for $x = 0.11$ and 0.29). Open stars, with corresponding sample labels, are values from the present work. Details of the structure of the $Ca_{3-x}Mg_x(PO_4)_2$ compound are drawn in the inset, with the substituted Ca5 site, allowing the crystallographic stabilization of the neighboring Ca4 site.

sented in Figure 2 in ref 35) and β-TCP (five nonequivalent Ca sites represented in Figure SI3 in ref 35). The seven possible sites were individually checked. The Mg occupancy factor was refined by constraining the alkaline-earth full occupancy of the site (Mg occupancy + Ca occupancy = 1), except for the Ca4 site in β-TCP, which presents a half-occupancy (Mg occupancy + Ca occupancy = $^1/_2$). Whatever the sample, no Mg atoms were localized in the HAp phase, in perfect agreement with the observations on the lattice parameters (Figures 1b and SI4b of the Supporting Information). The structure of HAp heated at 1100 °C is able to accept Ca substitution by a bigger alkaline earth as Sr (35, 36) but not by a smaller alkaline earth as Mg. The refined occupancy values for Mg in the Ca sites of the β-TCP phase can be found in the Supporting Information (Table SI2). Ca substitution by Mg is mainly realized in the Ca5 site (in agreement with ref 34), in contrast with substitution by Sr, which occurs mainly in the Ca4 site (35, 36). Only the sample 50Mg1100 shows also a weak substitution of Ca by Mg in the Ca3 site. In contrast with the results given by (34, 55), no indications were obtained concerning the substitution of Mg in the Ca4 site. The structural parameters of the Mg-doped β-TCP phase with composition β-$Ca_{2.841(9)}Mg_{0.159(9)}(PO_4)_2$ from the 50Mg1100 sample can be found in the Supporting Information (Table SI3). A comparison of the Ca−O interatomic distances and bond valence sums (BVSs) (57) for the five Ca sites for the pure β-TCP phase (43) and for the β-$Ca_{2.841(9)}Mg_{0.159(9)}(PO_4)_2$ phase from the 50Mg1100 sample is given in the Supporting Information (Table SI4). Average interatomic distances and BVSs agree well with the nonsubstitution (or very weak substitution) by Mg in the sites Ca1, Ca2, and Ca3, as well as with the evident Mg substitution in the site Ca5. The half-occupied Ca4 site is unusually coordinated to three oxygen atoms O9 belonging to the same phosphate (P1) tetrahedron (see the three broken bonds in the inset of Figure 4). A decrease of the average

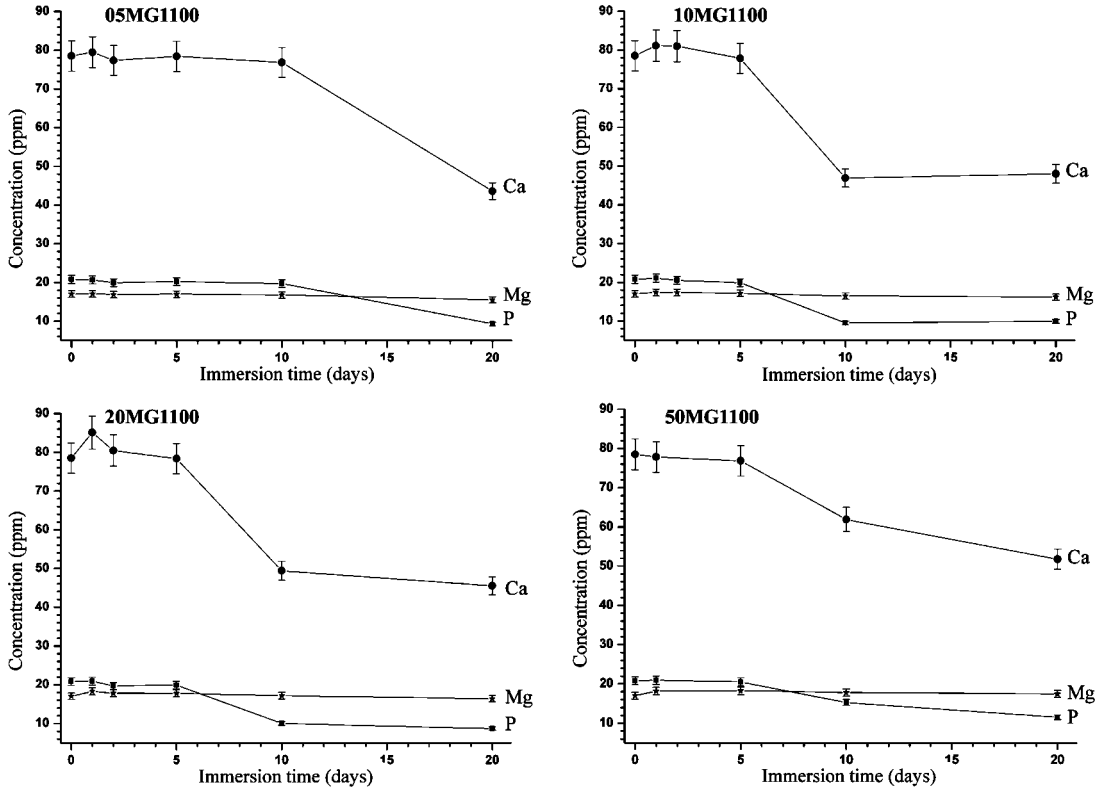

FIGURE 5. Evolution of the Ca (circles), Mg (stars), and P (squares) concentrations of the DMEM after immersion of the four Mg-substituted powdered samples calcined at 1100 °C.

⟨Ca4—O⟩ distances is observed but is not provided by Mg substitution in this Ca4 site. The Ca5 polyhedron has an octahedral coordination with no shared PO_4 edges (six neighboring O atoms belonging to six different PO_4 tetrahedra; see the inset in Figure 4). Ca4 and Ca5 polyhedra form the low-density column located on the 3-fold axis, described and named as the A column by Yashima et al. (43). Actually, the insertion of Mg atoms in the Ca5 sites results in the deformation of the Ca4 polyhedron with a closeness of Ca4 and O9 atoms (broken bonds in the inset of Figure 4), which allows an increase in the BVS of the Ca4 site. The BVS increases from 0.78 (pure β-TCP) to 1.29 (β-$Ca_{2.841(9)}Mg_{0.159(9)}(PO_4)_2$) for Ca4. A BVS value of 1.29 is still too weak for a divalent cation but widely better than 0.78. At the same time, the BVS value of the Ca5 site decreases from 2.73 (pure β-TCP) to 2.55 (β-$Ca_{2.841(9)}Mg_{0.159(9)}(PO_4)_2$). The doping stabilizing feature of the β-TCP structure is realized by improving the inappropriate situation of the Ca4 environment either by the direct substitution of a bigger alkaline earth (the case of the Sr^{2+} cation, which mainly substitutes the Ca4 site (35)) or by the substitution of a smaller alkaline earth in the neighboring Ca5 site of the low-density column (the present case of Mg^{2+}, which mainly substitutes in the Ca5 site).

3.5. Interaction with Biological Fluid. The effects of the Mg-substitution level (Figure 5) and the calcination temperature (Figure 6) on the interaction of BCP immersed in DMEM have been studied. The evolution of the Ca, Mg, and P concentrations in DMEM gives an indication of the dissolution of the BCP ceramic (i.e., increase of the concentrations in solution) and/or the precipitation at the surface of the BCP ceramic (i.e., decrease of the concentrations in solution). Figures 5 and 6 clearly show the precipitation of calcium phosphate depicted by a decrease of [Ca] and [P] when the immersion time increases. On the other hand, the Mg concentration is quite invariable. The higher the Mg-substitution level, the quicker the precipitation (Figure 5). For 05MG1100, the concentrations of all cations are constant during the first 10 days and the decreases of [Ca] and [P] are only observed after 20 days of immersion (Figure 5, top left). For the three other BCP ceramics calcined at 1100 °C, the decreases of [Ca] and [P] are already observable for an immersion time of 10 days. This gives an indication of a kinetically favored precipitation of a calcium phosphate layer at the surface of the Mg-substituted samples. The presence of Mg in the BCP ceramics appears to be beneficial for the in vitro behavior. The dissolution of the immersed powder can also be observed by the weak increase of the Mg concentration for the high-Mg-content samples (Figure 5, bottom), i.e., for the samples with a higher proportion of β-TCP and with a higher Mg content in the β-TCP phase. Despite the decrease of the solubility of β-TCP when increasing its magnesium content (37), in all of our samples, the Mg-substituted β-TCP phase still has a higher solubility than the HAp phase (because the maximal reached substitution corresponds to the $Ca_{2.751(9)}Mg_{0.249(9)}(PO_4)_2$ composition). It has been already mentioned that the in vitro bioactivity of HAp leads to the formation of a calcium phosphate layer, which contains a small amount of Mg (38). Then the presence of a Mg element in the β-TCP phase of BCP powders seems to accelerate the precipitation of this layer. The effect

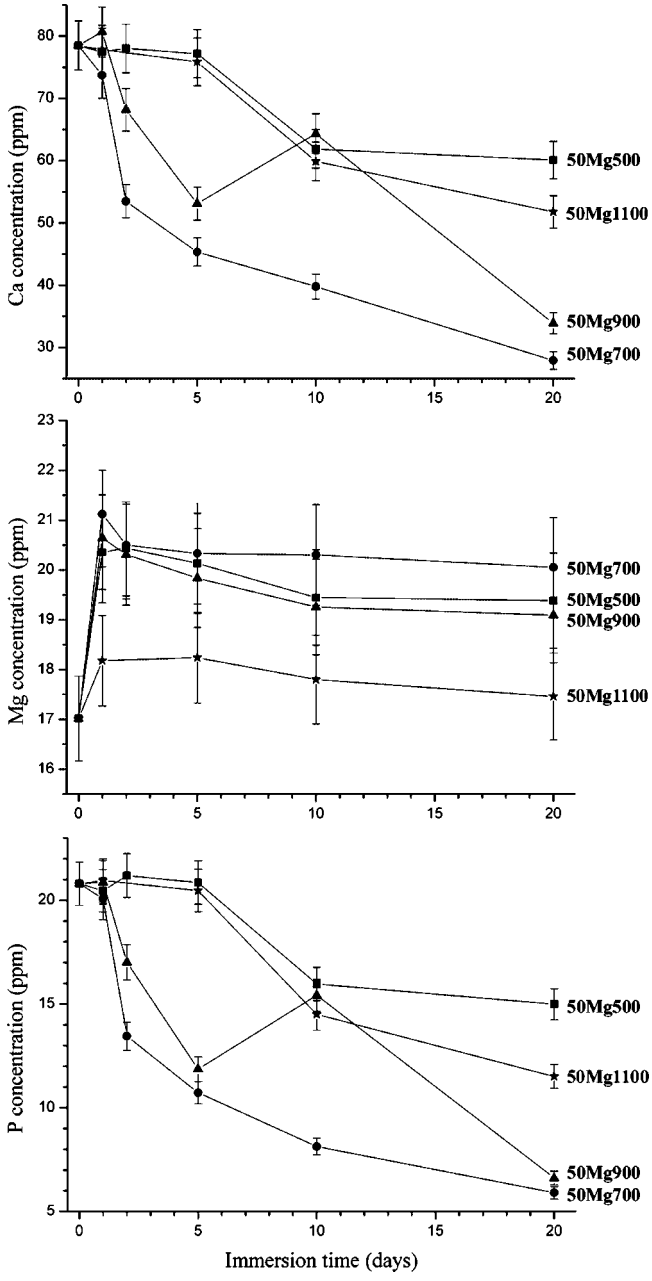

FIGURE 6. Evolution of the Ca (top), Mg (middle), and P (bottom) concentrations of the DMEM after immersion of 5 at. % of Mg-substituted powdered samples calcined at 500 (squares), 700 (circles), 900 (triangles), and 1100 (stars) °C.

of the calcination temperature (Figure 6) is correlated with the inserted Mg amount in the β-TCP phase. The Ca and P concentrations in DMEM are weaker after immersion of 50Mg700 compared to 50Mg500. Also, these concentrations are higher after immersion of 50Mg900 and even higher for 50Mg1100, compared to 50Mg700. This means that precipitation of the calcium phosphate layer is favored at the surface of the 50Mg700 sample (i.e., the sample that contains the less soluble and more stabilized Mg-substituted β-TCP phase). The solubility of the phases in BCP is not the most important feature to take into account to improve its bioactivity. The most important is the presence of nucleation sites at the crystallite surface, which are activated by the presence of inserted Mg atoms. The microstructural parameters, i.e., crystallinity and crystallite size, are certainly also important characteristics for the development of the biomimetic layer.

4. CONCLUSIONS

The sol−gel process has been used to prepare Mg-doped BCP ceramics. With respect to an unsubstituted sample, the Mg-substituted samples exhibit a higher proportion of the β-TCP phase, namely, at high temperature (above 1000 °C). The Mg substitution in BCP ceramics concerns only the β-TCP phase. No Mg substitution has been observed in the HAp phase (or a very weak substitution when a moderate temperature of calcination, 500 °C, is applied). The β-TCP weight amount in BCP is linearly dependent with the introduced Mg atomic amount for samples calcined at 1100 °C. The Mg-substituted β-TCP cell parameters agree fairly well with Vegard's law, and Mg^{2+} ions substitute for Ca^{2+} ions only in the Ca5 site at a low level of substitution. Such a stabilizing feature of Mg on the β-TCP structure is explained by an improvement of the environment of the Ca4 site. The Ca4 site, located on the 3-fold axis, is unusually face-coordinated to a phosphate tetrahedron. Electrostatic repulsion increases the interatomic Ca4−O distances, which leads to an extremely weak BVS. The Mg substitution of the neighboring Ca5 site allows one to decrease these three large Ca4−O bonds, which consequently leads to an improvment of the BVSs of both Ca4 and Ca5 sites. Such a stabilizing feature has been observed in the case of the Sr substitution. However, in the Sr case, the substitution is directly realized in the problematic Ca4 site because a big cation accommodates well the large Ca4−O distances and directly improves its BVS. From these results, it is clear that Mg substitution can be efficiently used to modulate the phase proportions of BCP and thus the behavior in solution of the material. Interactions of our Mg-substituted BCP ceramics with DMEM have shown an accelerating effect of Mg on the precipitation of the calcium phosphate layer at the surface of the powder. A moderate temperature of the calcination of 700 °C led to the best bioactivity properties. The effective partial substitution of Mg in β-TCP makes this material very interesting for orthopedic applications.

Acknowledgment. Financial support from the ANR under project Nanobonefiller (PNANO 2006) is gratefully acknowledged.

Supporting Information Available: Microstructural parameters refined for the HAp and β-TCP phases (Table SI1), Rietveld refinement results on the Mg insertion in the β-TCP structure (Table SI2), structural parameters of the Mg-doped β-TCP phase with composition β-$Ca_{2.841(9)}Mg_{0.159(9)}(PO_4)_2$ from the 50Mg1100 sample (Table SI3), comparison of the interatomic distances and the calculated BVSs for the pure and Mg-doped phases with composition β-$Ca_{2.841(9)}Mg_{0.159(9)}(PO_4)_2$ from the 50Mg1100 sample (Table SI4), Rietveld plot on the 5 wt % Mg-doped sample calcined at 700 °C, 50Mg700 sample ($\lambda = 1.5418$ Å) (Figure SI1), details of the PXRD patterns (in the range $20° < 2\theta < 60°$) from the Mg-free BCP series with calcination temperatures from 500 to 1100 °C (Figure SI2), Ca-substitution level in the Ca_{3-x}-

$Mg_x(PO_4)_2$ solid solution for the 50Mg series and for samples 20Mg1100 and 10Mg1100 (Figure SI3), and results of the Rietveld refinements as a function of the introduced Mg amount at 1100 °C, including quantitative phase analysis and unit volume per Ca = unit cell volume/unit cell number of Ca atoms (Figure SI4). This material is available free of charge via the Internet at http://pubs.acs.org.

REFERENCES AND NOTES

(1) Dahl, S. G.; Allain, P.; Marie, P. J.; Mauras, Y.; Boivin, G.; Ammann, P.; Tsouderos, Y.; Delmas, P. D.; Christiansen, C. *Bone* **2001**, *28*, 446.
(2) Lagier, R.; Baud, C.-A. *Pathol., Res. Pract.* **2003**, *199*, 329.
(3) Lee, R. S.; Kayser, M. V.; Ali, S. Y. *J. Anat.* **2006**, *208*, 13.
(4) Elliot, J. C. *Structure and Chemistry of the Apatites and Other Calcium Orthophosphates*; Elsevier: Amsterdam, The Netherlands, 1994.
(5) LeGeros, R. Z.; Lin, S.; Rohanizadeh, R.; Mijares, D.; LeGeros, J. P. *J. Mater. Sci. Mater. Med.* **2003**, *14*, 201.
(6) Livingston Arinzeh, T.; Tran, T.; Mcalary, J.; Daculsi, G. *Biomaterials* **2005**, *26*, 3631.
(7) Bouler, J. M.; Trecant, M.; Delecrin, J.; Royer, J.; Passuti, N.; Daculsi, G. *J. Biomed. Mater. Res.* **1996**, *32*, 603.
(8) Ergun, C.; Webster, T. J.; Bizias, R.; Doremus, R. H. *J. Biomed. Mater. Res.* **2002**, *59*, 305.
(9) Creedon, A.; Flynm, A.; Cashman, A. *Br. J. Nutr.* **1999**, *82*, 63.
(10) Kannan, S.; Lemos, I. A. F.; Rocha, J. H. G.; Ferreira, J. M. F. *J. Solid State Chem.* **2005**, *178*, 3190.
(11) Rude, R. K. *J. Bone Miner. Res.* **1998**, *13*, 749.
(12) Serre, C. M.; Papillard, M.; Chavassieux, P.; Voegel, J. C.; Boivin, G. *J. Biomed. Mater. Res.* **1998**, *42*, 626.
(13) Tsuboi, S.; Nakagaki, H.; Ishiguro, K.; Kondo, K.; Mukai, M.; Robinson, C.; Weatherell, J. A. *Calcif. Tissue Int.* **1992**, *50*, 34.
(14) Fondel, C.; Prien, E. L. *Science* **1946**, *103*, 326.
(15) Jensen, A. T.; Rowles, S. L. *Acta Odontol. Scand.* **1957**, *16*, 121.
(16) LeGeros, R. Z.; LeGeros, J. P. Phosphate minerals in human tissues. In *Phosphate minerals*; Nriagu, J. O., Moore, P. B., Eds.; Springer: Berlin, pp 351−355.
(17) Ryan, L. M.; Cheung, H. S.; LeGeros, R. Z.; Kurup, I. V.; Toth, J.; Westfall, P. R.; McCarthy, G. M. *Calcif. Tissue Int.* **1999**, *65*, 374.
(18) Klein, C. P. A. T.; Driessen, A. A.; De Groot, K. *J. Biomed. Mater. Res.* **1983**, *1*, 7–769.
(19) Klein, C. P. A. T.; De Groot, K.; Driessen, A. A.; Van der Lubbe, H. B. M. *Biomaterials* **1986**, *7*, 144.
(20) Dhert, W. J. A.; Klein, C. P. A. T.; Jansen, J. A.; Van der Velde, E. A.; Vriesde, R. C.; Rozing, P. M.; De Groot, K. *J. Biomed. Mater. Res.* **1993**, *2*, 7–127.
(21) LeGeros, R. Z.; Daculsi, G.; Kijkowska, R.; Kerebel, B. The effect of magnesium on the formation of apatites and withlockites. In *Magnesium in Health and Disease*; Itokawa, Y., Durlach, J., Eds.; John Libbey and Co., Ltd.: New York, 1989.
(22) Bigi, A.; Foresti, E.; Gregorini, R.; Ripamonti, A.; Roveri, N.; Shah, J. S. *Calcif. Tissue Int.* **1992**, *50*, 439.
(23) Boskey, A. L.; Rimnac, C. M.; Bansal, M.; Federmann, M.; Lian, J.; Boyan, B. D. *J. Orthop. Res.* **1992**, *10*, 774.
(24) Montel, G.; Bonel, G.; Heughebaert, J. C.; Trombe, J. C.; Rey, C. *J. Cryst. Growth* **1981**, *53*, 74.
(25) Hamad, M.; Heughebaert, J. C. *J. Cryst. Growth* **1986**, *79*, 192.
(26) Hamad, M.; Heughebaert, J. C. *J. Chim. Phys.* **1987**, *84*, 985.
(27) Ben Abdelkader, S.; Khattech, I.; Rey, C.; Jemal, M. *Thermochim. Acta* **2001**, *376*, 25.
(28) Suchanek, W. L.; Byrappa, K.; Shuk, P.; Riman, R. E.; Janas, V. F.; Ten Huisen, K. S. *Biomaterials* **2004**, *25*, 4647.
(29) Gibson, I. R.; Bonfield, W. *J. Mater. Sci. Mater. Med.* **2002**, *13*, 685.
(30) Fadeev, I. V.; Shorneva, L. I.; Barinov, S. M.; Orlovskii, V. P. *Inorg. Mater.* **2003**, *39*, 947.
(31) LeGeros, R. Z. Calcium phosphates in oral biology and medicine. In *Monographs in Oral Science*; Myers, H. M., Ed.; Karger: Basel, Switzerland, 1991; Vol. 15.
(32) Ishikawa, K.; Ducheyne, P.; Radin, S. *J. Mater. Sci. Mater. Med.* **1993**, *4*, 165.
(33) Dickens, B.; Schroeder, L. W.; Brown, W. E. *J. Solid State Chem.* **1974**, *10*, 232.
(34) Schroeder, L. W.; Dickens, B.; Brown, W. E. *J. Solid State Chem.* **1977**, *22*, 253.
(35) Renaudin, G.; Laquerrière, P.; Filinchuk, Y.; Jallot, E.; Nedelec, J. M. *J. Mater. Chem.* **2008**, *18*, 3593.
(36) Renaudin, G.; Jallot, E.; Nedelec, J. M. *J. Sol−Gel Sci. Technol.* **2008**, in press.
(37) Li, X.; Ito, A.; Sogo, Y.; Wang, X.; LeGeros, R. Z. *Acta Biomater.* **2009**, *5*, 508.
(38) Jallot, E.; Nedelec, J. M.; Grimault, A. S.; Chassot, E.; Laquerriere, P.; Grandjean-Laquerriere, A.; Laurent-Maquin, D. *Colloids Surf.* **2005**, *B 42*, 205.
(39) Grandjean-Laquerriere, A.; Laquerriere, P.; Jallot, E.; Nedelec, J. M.; Guenounou, M.; Laurent-Maquin, D.; Philips, T. *Biomaterials* **2006**, *27*, 3195.
(40) Nedelec, J. M.; Courtheoux, L.; Jallot, E.; Lao, J.; Kinowski, C.; Laquerriere, P.; Mansuy, C.; Renaudin, G.; Turrell, S. *J. Sol−Gel Sci. Technol.* **2008**, *46*, 259.
(41) Rodriguez-Carvajal, J. *PROGRA M FullProf.2k*, version 3.20; Laboratoire Léon Brillouin (CEA-CNRS): France, 2005 (*FullProf.2k* manual available on http://www-llb.cea.fr/fullweb/fp2k/fp2k_divers.htm). See also: Rodriguez-Carvajal, J., Roisnel, T. EPDIC-8, Uppsala, Sweden, May 23−26, 2002; Materials Science Forum 123; Trans. Tech. Publication Ltd.: Zurich, Switzerland, 2004; p 443.
(42) Rodriguez-Lorenzo, L. M.; Hart, J. N.; Gross, K. A. *J. Phys. Chem. B* **2003**, *107*, 8316.
(43) Yashima, M.; Sakai, A.; Kamiyama, T.; Hoshikawa, A. *J. Solid State Chem.* **2003**, *175*, 272.
(44) Ganguly, R.; Siruguri, V.; Gopalakrishnan, I. K.; Yakhmi, J. V. *J. Phys.: Condensed Matter* **2000**, *12*, 1283.
(45) Bragg, W. L. *Nature* **1920**, *105*, 646.
(46) Chessin, H.; Hamilton, W. C.; Post, B. *Acta Crystallogr.* **1965**, *18*, 689.
(47) Calvo, C. *Inorg. Chem.* **1968**, *7*, 1345.
(48) Boudin, S.; Grandin, A.; Borel, M. M.; Leclaire, A.; Raveau, B. *Acta Crystallogr.* **1993**, *C49*, 2062.
(49) François, M.; Renaudin, G.; Evrard, O. *Acta Crystallogr.* **1998**, *C54*, 1214.
(50) Renaudin, G.; François, M. *Acta Crystallogr.* **1999**, *C55*, 835.
(51) Renaudin, G.; Rapin, J.-P.; Humbert, B.; François, M. *Cem. Concr. Res.* **2000**, *30*, 307.
(52) Parodi, J. A.; Hickok, R. L.; Segelken, W. G.; Cooper, J. R. *J. Electrochem. Soc.* **1965**, *112*, 688.
(53) Bian, J.-J.; Kim, D.-W.; Hong, K.-S. *Mater. Lett.* **2004**, *58*, 347.
(54) Renaudin, G.; Bertrand, A.; Dubois, M.; Gomes, S.; Chevalier, P.; Labrosse, A. *J. Phys. Chem. Solids* **2008**, *69*, 1603.
(55) Bigi, A.; Falini, G.; Foresti, E.; Ripamonti, A.; Gazzano, M.; Roveri, N. *Z. Kristallogr.* **1996**, *211*, 13.
(56) Dickens, B.; Brown, W. E. *TMPM, Tschermaks Mineral. Petrogr. Mitt.* **1971**, *16*, 79.
(57) Brese, N. E.; O'Keefe, M. *Acta Crystallogr.* **1991**, *B47*, 192.

AM800162A